Na-Cellulose Formation in a Single Cotton Fiber Studied by Synchrotron Radiation Microdiffraction

J. Schoeck, R. J. Davies, A. Martel, and C. Riekel*

European Synchrotron Radiation Facility, B.P. 220, F-38043 Grenoble Cedex, France

Received September 1, 2006; Revised Manuscript Received November 26, 2006

A cotton fiber was kept under slight tension and exposed locally to a stream of aqueous 1 N NaOH microdrops of 50 μm diameter. The resulting "macrodrop" of about 300 μm size was at the origin of the formation of Na-cellulose I domains extending about 550 μm from the center of the macrodrop along the fiber. The phase transformation zone between cellulose I and Na-cellulose I was mapped by scanning synchrotron radiation microdiffraction using a 300 nm × 300 nm beam. A stitching technique was used to limit radiation damage. Subsequent exposure of the NaOH containing macrodrop to a stream of H_2O or HCl microdrops converted part of the Na-cellulose I back into cellulose I.

Introduction

The transformation of cellulose I into cellulose II by aqueous NaOH is a commercial process known as "mercerization". Mercerized cotton fibers exhibit a more appealing luster and greater tensile strength, and they uptake dye more easily than their untreated counterparts. The conversion of cellulose during mercerization involves at least one (possibly more) intermediate Na-cellulose crystalline phases (e.g., Na-cellulose I)[1−9] in which sodium ions intercalate between sheets of cellulose chains.[7] It is during this step that the parallel-chain structure of cellulose I is thought to convert into the antiparallel-chain structure of cellulose II.[7] For this reason, the intermediate phases are of particular interest, both from an academic and commercial perspective.

To date, the primary techniques employed for studying structural transitions in cellulose are electron and X-ray diffraction (ED and XRD, respectively). However, these methods both have significant limitations for fiber-related studies. ED provides a high spatial resolution but requires the embedding and sectioning of fiber samples.[2,4] Consequently, it is not suitable for studying phase changes in situ. On the other hand, while XRD and (traditional) synchrotron radiation diffraction offer extensive in-situ possibilities, they lack the spatial resolution of ED.[10−12] They are confined therefore to studying large fiber bundles from which the experimental results are dominated by averaging.

As an alternative to ED and XRD, synchrotron radiation microdiffraction combines the main advantages of both techniques. It offers the in-situ capability of X-rays with the benefit of a high spatial resolution.[13−16] This makes it suitable for studying phase changes in situ within single fiber volumes. This applicability is demonstrated in the present study which reports on the first use of this technique for studying the onset of Na-cellulose formation in single cotton fibers. In this case, the formation of Na-cellulose is initiated locally using microdrop technology.[17] In addition, the article will also address instrumental issues and image treatment of large data sets and discuss future experimental possibilities.

* Author to whom correspondence should be addressed. E-mail: riekel@esrf.fr.

Experimental Section

Materials. Cotton boll fibers were cleaned by refluxing twice in a mixture of ethanol and toluene (60/40 v/v) for 4 h. This removed the waxy component, after which the fibers were air-dried. Single fibers were selected with tweezers under an optical microscope and attached using cyanoacrylate adhesive to a cardboard frame. The frame was then attached to a custom built tensile stage comprising a linear motor and a force sensor. This enabled the fiber to kept under slight tension (0.4−0.8 g force), to stabilize its position in the microbeam for extended periods. During the in-situ experiment, fibers were exposed locally to 1 N NaOH, H_2O, or 0.5 N HCl microdrops at room-temperature using a microdrop generator (described below). Solutions were prepared using deionized water and were microfiltered before insertion into the device to avoid clogging.

For the ex-situ experiment, a bundle of cotton fibers was immersed for 6 h in 5 N NaOH in order to get a conversion into Na-cellulose I without external constraints. Neutralization of the Na-cellulose I was performed by washing with 1 N HCl for 60 h.

Microdrop Generator. Microdrops were generated by a drop-on-demand system based on a microdrop-head. This consists of a glass capillary mounted concentrically in a piezoelectric actuator.[17−20] The microdrop diameter is defined by the drop-head capillary exit. This is about 50 μm in this case, with a relative change in volume between consecutive microdrops of ±1%. (company specifications). With such drop diameters, and droplet speeds of about 2 m/s, surface energies dominate with respect to kinetic energy. Consequently, microdrops do not splash on impact making a highly localized delivery system.[17] Figure 1A shows the microdrop-head installed above a fiber which is fixed to the tensile stage. The distance between the capillary exit of the microdrop-head and the surface of the fiber was approximately 300−400 μm. A microdrop frequency of ≤1 Hz allowed a constant supply of liquid to be directed at a chosen point on the fiber. The resulting "macrodrop" could then be maintained in suspension on the fiber (Figure 1B). Aqueous NaOH, diffusing from the macrodrop into the fiber, will become increasingly concentrated along its diffusion path as the fiber is permeable to H_2O vapor. The concentration limit for Na-cellulose formation, which is about 2.25 N for primary wall cellulose,[21] will therefore be superseded, and Na-cellulose I formation will occur. After stopping the microdrop generator, the macrodrop volume will be reduced gradually by evaporation until a Na_2CO_3 crust is formed on its surface by reaction of NaOH with CO_2 from air (Figure 1C).

To change the microdrop solution, the microdrop-head can be replaced which takes around 30 min. Alignment of the fiber to the

10.1021/bm060844w CCC: $37.00
Published on Web 01/27/2007

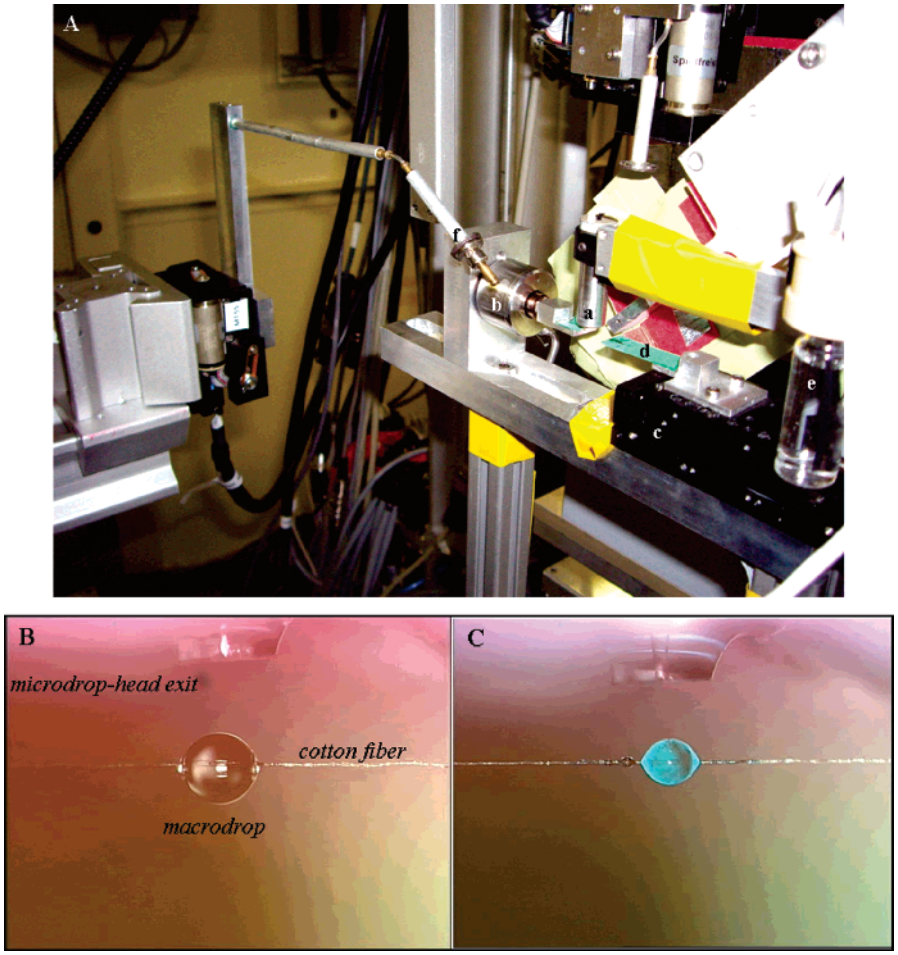

Figure 1. (A) Tensile stage and microdrop generator: (a) microdrop-head; (b) force sensor; (c) translation stage of tensile stage; (d) cardboard frame carrying single cotton fiber; (e) liquid reservoir of microdrop generator; (f) motorized beamstop support. (B) Capillary exit of microdrop-head positioned above cotton fiber. A macrodrop of 1 N aqueous NaOH has accumulated on the fiber during dropping. (C) Aqueous NaOH macrodrop after water evaporation; a solid crust of NaOH_H_2O has formed on its surface. Pictures recorded with the beamline microscope.

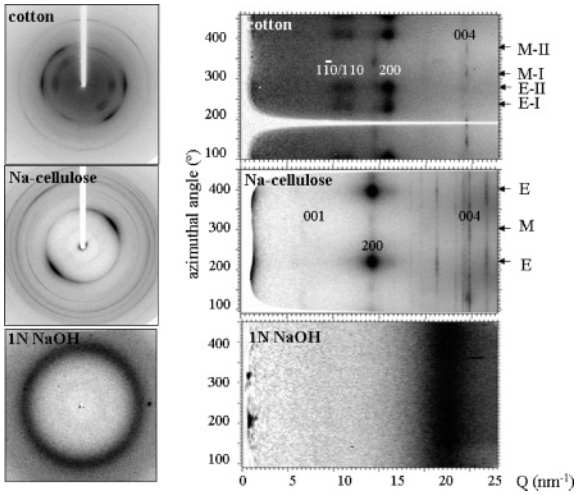

Figure 2. The left panel shows selected patterns of cotton fiber, Na-cellulose I from cotton fiber, and 1 N NaOH solution from macrodrop (Figure 1B). The cotton (cellulose I) and Na-cellulose I patterns were recorded with a 5 × 5 μm^2 beam and the aqueous NaOH pattern with a 300 × 300 nm^2 beam. The right panel shows cake regrouped patterns shown to the left. Abbreviations: M, meridian; E, equator. Note the split pattern of the cotton fiber.

microdrop-head involved translating the fiber through the droplets' path until the macrodrop was observed. The control unit of the microdrop generator was triggered by a TTL (transistor−transistor logic) signal from a VME (virtual machine environment) frequency generator board. Software control was possible through a SPEC interface (Certified Scientific Software) running on a Unix based workstation.[20]

Synchrotron Radiation Experiments. Synchrotron radiation experiments were performed at the ESRF-ID13 beamline.[14] A monochromatic beam of $\lambda = 0.097$ nm was focused to a 300 × 300 nm^2 spot at the sample position by crossed, linear Fresnel lenses.[22] The sample-to-detector distance was calibrated by an Al_2O_3 powder standard. Additional diffraction patterns were also collected using a 5 × 5 μm^2 beam, generated by the combination of Be refractive lenses[23] and collimator at the ID13 microgoniometer.[24]

The microdrop generator and tensile stage were attached to the ID13 beamline's *x*/*y*/*z* scanning stage. Prior to the start of the experiment, the fiber was aligned to the microbeam's position using an on-axis optical microscope. For data collection, mesh-scans were performed around selected areas of the sample and diffraction patterns recorded by a 16-bit MARCCD165 detector (MAR USA). The detector's 2K × 2K pixels were binned to 1K × 1K in order to reduce the readout time per pattern to about 3 s. Each pattern was recorded with constant monitor counting, which compensates for beam current fluctuations. Exposure times per pattern were between 500 ms and 1 s in order to limit radiation damage, which was similar to that observed for starch granules.[19] It was not possible to perform mesh-scans with a step-width corresponding to the beam size due to radical generation and propagation. This results in the rapid failure of fibers under tension. Instead, a beam "stitching" technique was used with a step-width of several micrometers to permit the fiber to be scanned twice (consecutively).

Individual diffraction patterns were displayed and analyzed using the software package FIT2D.[25] For background reduction, a pattern recorded during a mesh-scan outside the sample area was subtracted.

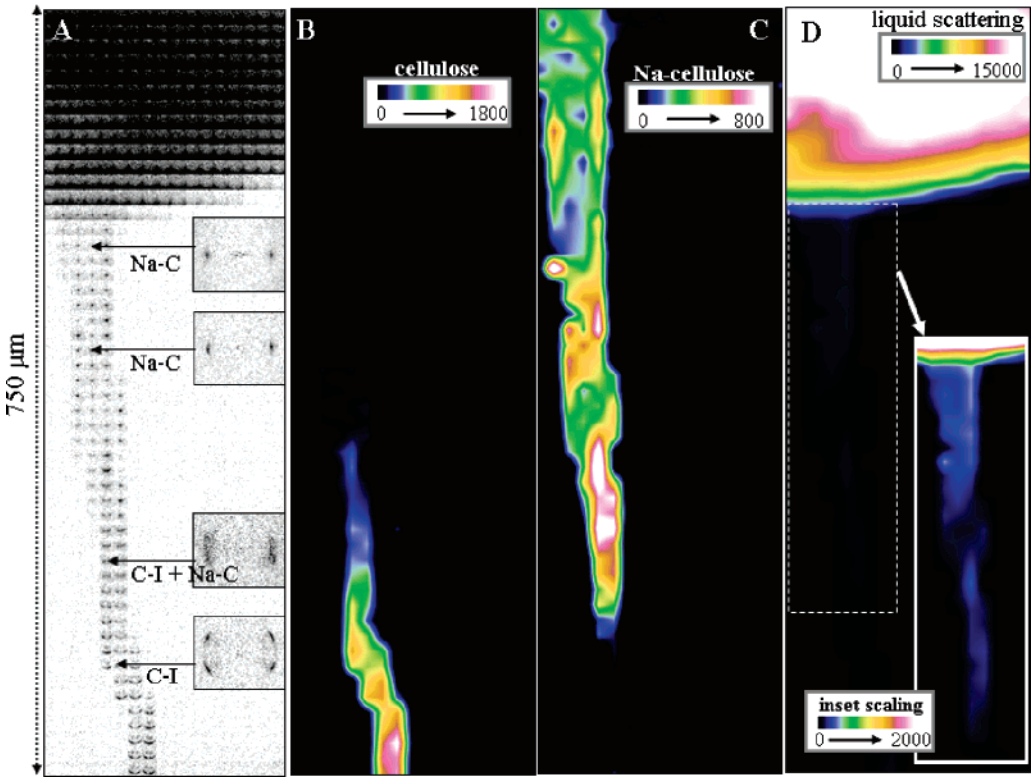

Figure 3. (A) Composite image based on "pixels" limited in reciprocal space extension to the cellulose I and Na-cellulose I 200 reflections. The contours of the fiber and the macrodrop are visible. Note that the fiber axes of individual pixels are rotated by 90° to the macroscopic fiber axis. Selected "pixels" with the correct orientation of the fiber axes and covering a larger range have been highlighted. Abbreviations: C-I, cellulose I; Na-C, Na-cellulose I. (B) Interpolated composite image showing integrated intensity of cellulose I 200 reflection. (C) Same for Na-cellulose 200 reflection. (D) Same for liquid scattering peak.

Typical patterns of cellulose I, Na-cellulose, and 1 N NaOH solution are collected in Figure 2. The Na-cellulose pattern shown was recorded from a fully converted cotton fiber glued to a glass capillary. The patterns to the right have been cake-regrouped for displaying against a Q-scale ($Q = 4\pi \sin \Theta)\lambda^{-1}$). Recursive data analysis of large pattern series was carried out using specialist batch processing software.[26] Apparent particle size (L) was calculated via the Scherrer formula.[27] Instrumental line broadening was determined by an Al_2O_3 powder standard and taken into account when calculating particle sizes.

Results and Discussion

Na-Cellulose Formation. A single cotton fiber was exposed to 1 N NaOH microdrops for 165 s resulting in the formation of a macrodrop with a size of about 300 μm along the fiber axis (Figure 1B). The microdrop generator was then stopped and a mesh-scan started over an area of $750_h \times 80_v$ μm^2 with a mesh resolution of $15_h \times 5_v$ μm^2 and approximately 0.5 s exposure per pattern. The scan was started in a horizontal direction, 750 μm from the macrodrop's center. The resulting data set containing 867 frames took approximately 1 h to collect. Figure 3A shows a composite image showing each diffraction pattern arranged according to its position within the mesh scan. Each pattern is cropped around the position of the cellulose I and Na-cellulose I 200 reflections.[7,28] This allows the contours of the fiber to be discerned. The position of the macrodrop is also visible in relation to the scan region. This is due to tail contributions from the strong liquid scattering background close to the 200 reflection position (Figure 2). Several scan positions are selected in Figure 3A and are shown to the right in greater detail over extended reciprocal space. These show the transition from a split cellulose fiber pattern to a mixed cellulose/Na-cellulose pattern, and finally to a single fiber pattern of Na-cellulose.

In order to better show how these phases vary throughout the scan region, Figure 3B shows the spatial distribution of cellulose I, calculated from the integrated intensity of the cellulose I 200 contribution. This is determined from the total scattering intensity within 90° segments centered both radially and azimuthally around the 200 maxima, covering the entire peak. Other isotropic contributions were eliminated by subtracting the same Q-range, azimuthally offset by 90° from each segment.[26] Figure 3C shows a similar "phase map" calculated in the same way for the 200 reflection of Na-cellulose. Finally, Figure 3D shows the distribution of liquid, calculated from the integrated intensity of the liquid scattering peak. In addition to the spatial distribution of each phase, these composite diagrams show the transformation zone between cellulose and Na-cellulose. One can thus follow Na-cellulose formation into the center of the microdrop (Figure 3C). It is interesting to note that the intensity of the Na-cellulose 200 reflection increases outside the macrodrop region, up to the limit of its phase range (Figure 3C). Meanwhile, liquid scattering seems to be weak from within the fiber and is limited to the Na-cellulose phase range (Figure 3D).

While the split fiber pattern gradually changes into a single fiber pattern, across the fiber diameter patterns are nearly invariant (Figure 3A). This allows data analysis to be simplified and counting statistics increased by reducing the 2D composite image (Figure 3A) to a single line of patterns. Thus, individual patterns containing fiber scattering were summed in rows normal to the fiber axis, and the corresponding (also summed)

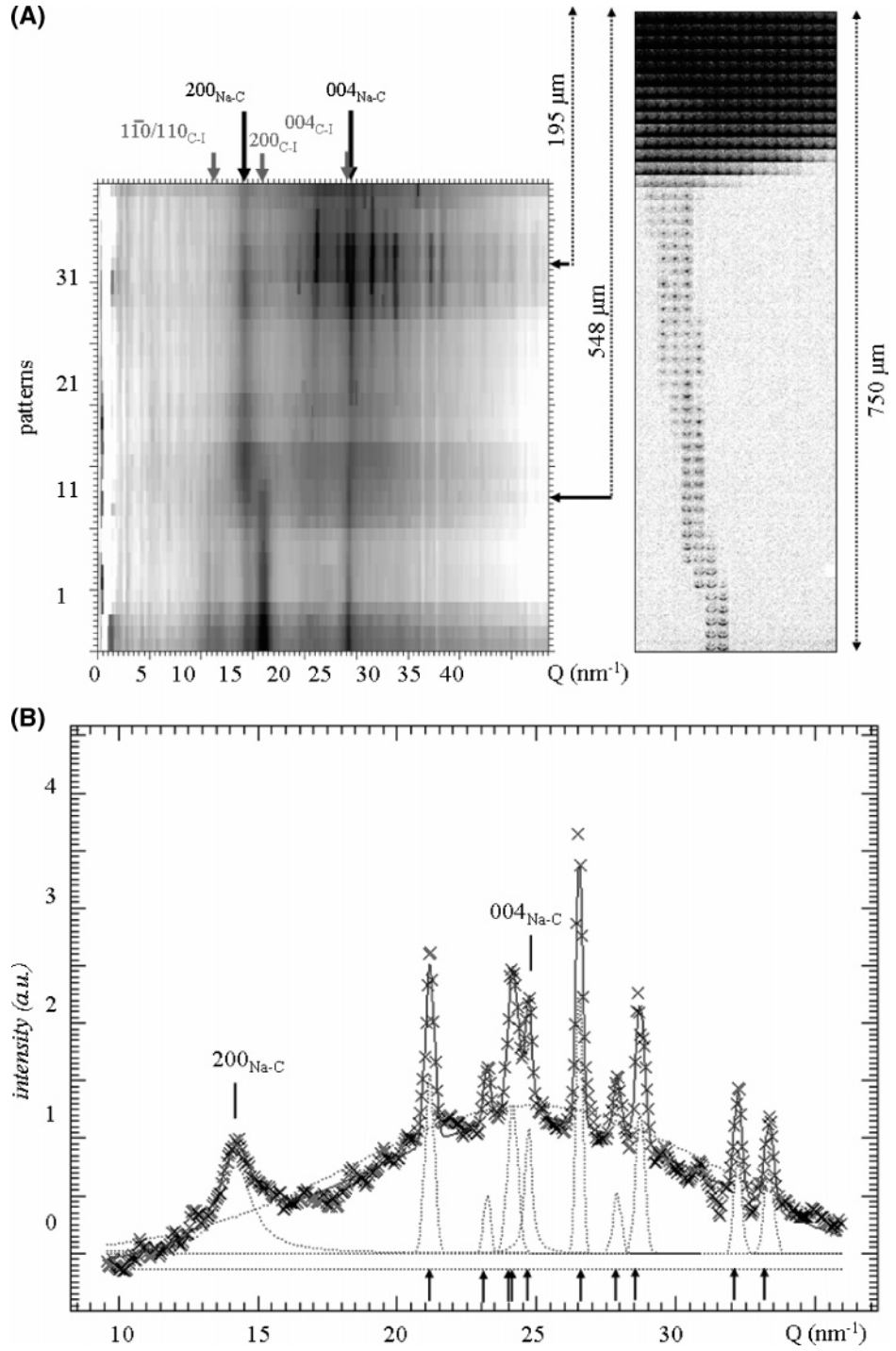

Figure 4. (A) Composite image based on 1D intensity profiles corresponding to sequence of azimuthally averaged fiber diffraction patterns, which were obtained by summing patterns normal to the macroscopic fiber direction (Figure 3). The distances of the zones of Na_2CO_3 precipitation and the cellulose I/Na-cellulose phase transformation from the center of the macrodrop are indicated. The composite image on the right has been scaled in length to the line of patterns; step increment between successive patterns: 15 μm. (B) Azimuthally averaged scattering pattern recorded close to macrodop showing the Na-cellulose I 200 reflection and several Na_2CO_3 reflections sitting on a broad background due to residual liquid scattering. Peak fits (solid lines) are based on Lorentzian profiles for Na-cellulose, Gaussian profiles for Na_2CO_3 peaks and liquid scattering and a 0-order polynomial background. The position of the Na_2CO_3 peaks from literature[29] is indicated by arrows.

background patterns were subtracted. For analysis, the patterns were azimuthally or radially averaged. A projection of the sequence of azimuthally averaged patterns shows the transition zone (via the cellulose I and the Na-cellulose 200 reflections) to be about 550 μm from the macrodrop center (Figure 4A). A series of Na_2CO_3 reflections[29] are also observed about 195 μm from the macrodrop center, superimposed on a broad diffuse peak attributable to residual liquid scattering (Figures 3D and 4B). This can be explained as Na_2CO_3 crystallites precipitating at the edge of the retreating macrodrop. This is due to H_2O evaporation which results in supersaturation at about 16.3 N NaOH[2] and a reaction of the solid NaOH with CO_2 from air.

Further details of the transformation can be deduced from a least-squares fit to the azimuthally averaged patterns.[25] Lorentzian profiles were used due to their previous application to native cellulose,[30,31] with a zero-order polynomial background for patterns dominated by cellulose scattering. However, a first-order polynomial background was required for patterns domi-

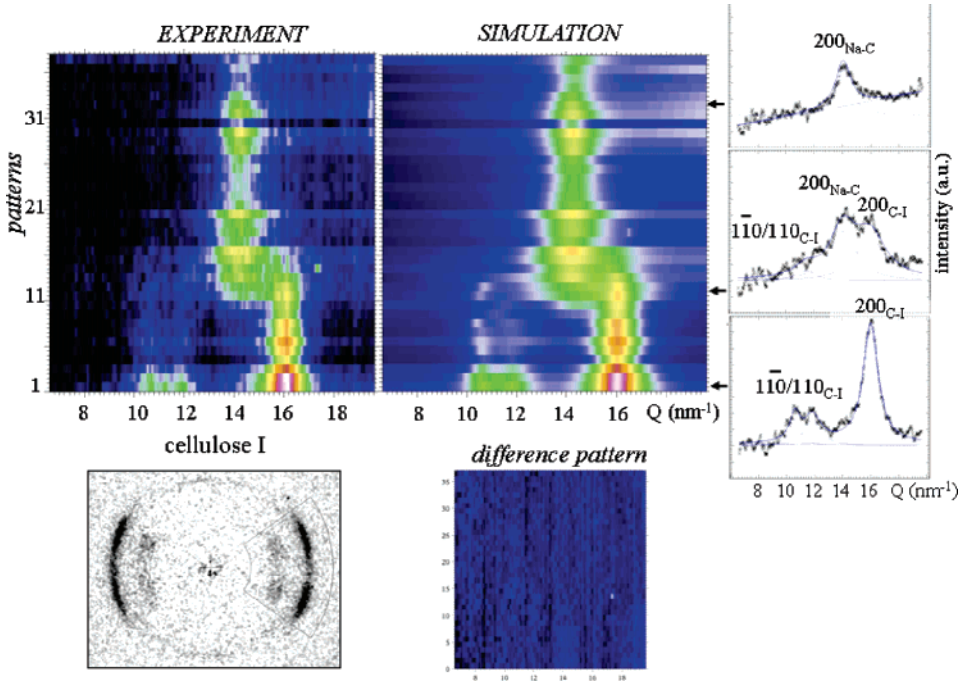

Figure 5. Composite image corresponding to sequence of azimuthally integrated intensity distributions covering the range of the cellulose 1$\bar{1}$0/110; 200 reflections and of the Na-cellulose 200 reflection; sequence as for Figure 4A. The azimuthal range used is shown for a cellulose I pattern. Step increment between successive patterns: 15 μm. The intensity fluctuation for the individual peaks along the fiber axis might be due to the "stitching" technique used in data collection as the twisting of the cotton fiber implies changes in scattering volumes for the 300 $\times$ 300 nm^2 beam. The experimental patterns are compared with the simulated patterns to the right. Simulations are based on Lorentzian profiles for cellulose I and Na-cellulose I 200 reflections and a zero-order or first-order polynomial background depending on the position in the fiber (see text). Selected profile fits are shown to the very right (blue lines correspond to fitted curves). The difference map between experimental and simulated data is shown below. Abbreviations: C-I, cellulose I; Na-C, Na-cellulose I.

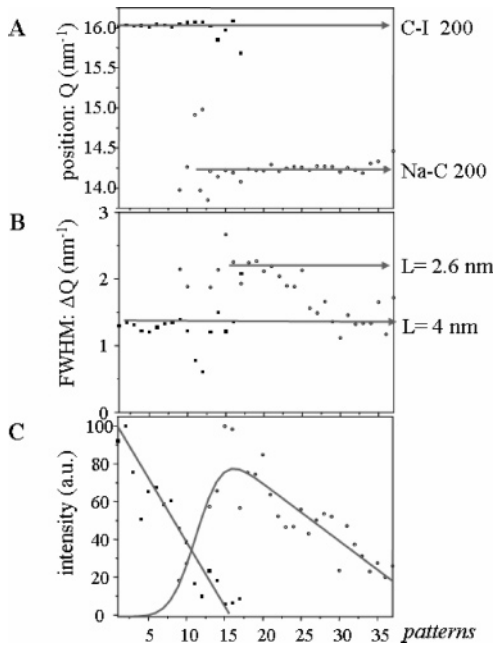

Figure 6. Evolution of profile parameters of the cellulose I (■) and Na-cellulose I 200 (○) reflections. (A) Peak position (Q, nm^{-1}). (B) Full-width-half-maximum (fwhm: ΔQ(nm^{-1})). (C) Integrated intensity. The lines in the peak position and fwhm plots are guides to the eye. The intensity variation of the cellulose 200 reflection has been fitted by a linear regression curve (line). The intensity variation of the Na-cellulose I 200 reflection has been fitted by a model (line) as explained in the text. The particle size (L) was calculated via the Scherrer formula.[27]

nated by Na-cellulose, due to the tail contribution from liquid scattering in the fiber (Figure 2). The variation in radial intensity as a function of position along the fiber axis is shown in Figure 5. This corresponds to a radial range covering the most intense equatorial reflections of cellulose and Na-cellulose, as shown for the cellulose I pattern in Figure 5. The experimental data can be fully simulated by assuming Lorentzian profiles for the cellulose 1$\bar{1}$0/110/200 reflections and for the Na-cellulose 200 reflection. The Lorentzian fits (blue lines) are shown for selected intensity profiles in Figure 5 to the right. The difference map between experimental and simulated data is practically featureless (Figure 5). The key individual fit parameters of cellulose and Na-cellulose 200 reflections are shown in Figure 6. These results suggest that the phase transformation can be described by coexisting cellulose and Na-cellulose domains. Complete conversion to Na-cellulose has taken place outside the phase transformation range on the side of the macrodrop. The apparent particle sizes (L's) of the cellulose and Na-cellulose domains, determined via the Scherrer formula from the 200 reflections, are both $L \approx 4$ nm outside the phase transformation zone.

Starting from the very end of the fiber, a decrease is apparent in the intensity of the 200 cellulose reflection before the appearance of the Na-cellulose 200 reflection (Figures 5 and 6). In the absence of an additional phase contribution or short-range order, it is tentatively suggested that cellulose crystalline domains are randomly intercalated by NaOH with a loss of long range order. In the zone of the phase transformation, a significant reduction is observed in the size of Na-cellulose domains ($L \approx$ 3 nm), which increases gradually to $L \approx 4$ nm toward the macrodrop. This would be in agreement with the proposed mechanism of a nucleation/growth process in the amorphous parts between nanocrystalline domains.[32]

It is not clear whether the amorphous phase suggested in this work corresponds to one of the amorphous phases described previously.[33,34] In particular, it is not completely excluded that a second, short-range order phase could be associated with part

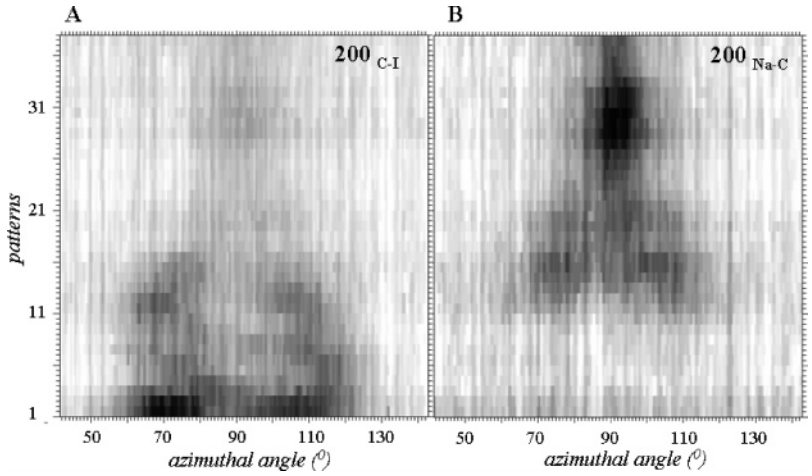

Figure 7. Composite image corresponding to projection of sequence of radially integrated azimuthal intensity distribution of 200 reflections, same sequence as for Figure 4A. The radial integration was performed within narrow radial peak profiles. (A) Cellulose 200 reflection. (B) Na-cellulose I 200 reflection. The weak scattering for cellulose I outside the phase transformation is due to the tails of the Na-cellulose peak. Particle size (*L*) calculation as for Figure 6.

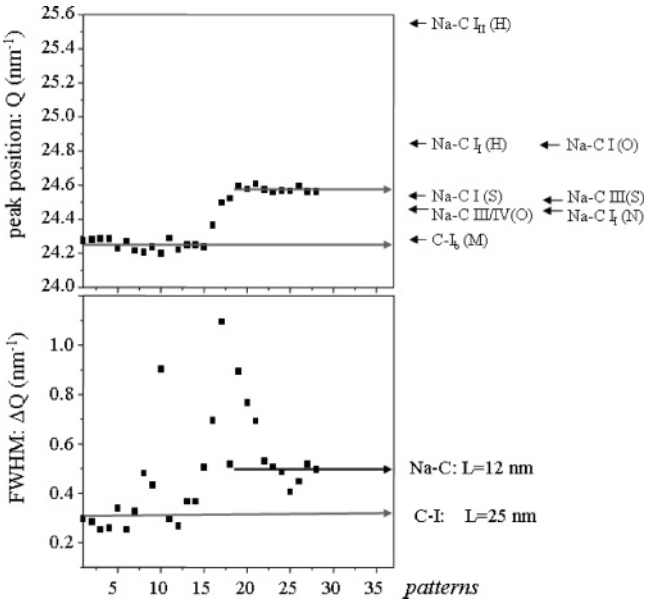

Figure 8. Observed positional change of 004 reflections compared with literature values of cellulose I and several Na-cellulose phases: C-I_b (M);[28] Na-C I_I/I_{II} (H);[35] Na-C I/III/IV (O);[2] Na-C I_I (N);[4] Na−C I/III (S).[40] The pattern sequence corresponds to Figure 4A. Note that some of the unit cells, e.g.,[40] require a doubling of the *c*-axis fiber repeat, which was neglected for better comparison. Additional overlapping peaks close to the macrodrop did not allow determining the 004 position beyond pattern 27. The lines are guides to the eye.

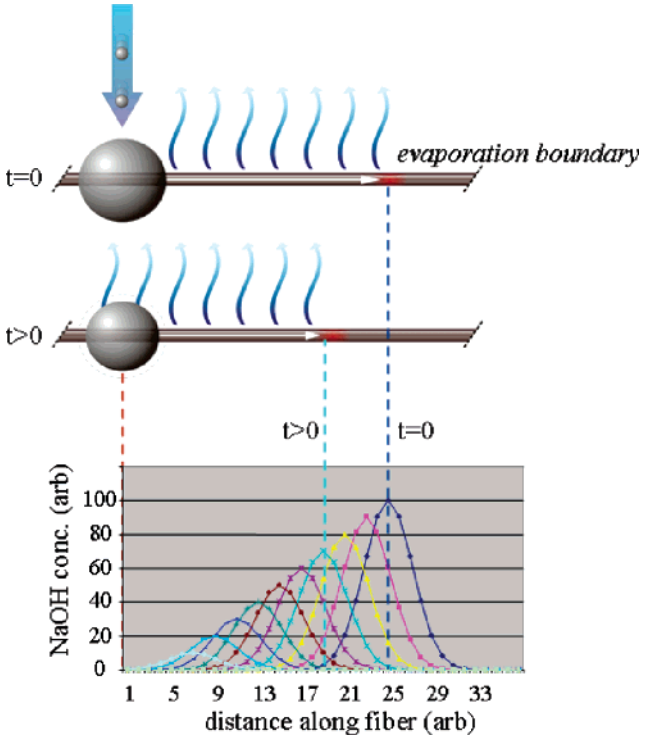

Figure 9. Model for development of a NaOH concentration gradient in the fiber (see text).

of the phase transformation, as a very broad Na-cellulose peak has to be fitted for 2 patterns in the transition range. It is interesting to note that the transition zone shown in Figure 5 bears a close resemblance with the transient phase observed for the β-chitin hydration, which can be modeled by statistical mixture of two lamellar phases.[18] A more detailed analysis would, however, require greater counting statistics and higher resolution mesh-scans. Nevertheless, the twisted cotton fiber morphology which yields the characteristic split cellulose pattern (Figure 2) must also be valid for a short-range order phase. This can be deduced from the azimuthal intensity distribution of cellulose and Na-cellulose 200 reflections (Figure 7A,B). The figure shows that the split fiber pattern is not modified at the onset of Na-cellulose formation. Thus, the Na-cellulose 200 reflection is also azimuthally split to begin with. However, this subsequently becomes a single peak outside of the transformation range. This suggests that a critical concentration of Na-cellulose domains is required before local fiber twisting can be overcome. There is therefore no evidence for an isotropic amorphous phase, deduced from Raman microprobe data.[34]

The evolution of the 004 layer line position and its full-width at half-maximum (fwhm) determined by Lorentzian fits is shown in Figure 8. Although a slight positional shift is visible between cellulose and Na-cellulose in Figure 4, it is not possible to separate this into two components. The fit of two closely neighboring peaks by a single Lorentzian explains the systematic increase of the fwhm in the two phase range. The apparent particle sizes derived from the 004 reflections can, however, be determined from the single phase ranges and show that the *c*-axis length of Na-cellulose domains is smaller than for cellulose (cellulose I, $L \approx 25$ nm; Na-cellulose, $L \approx 12$ nm). The peak position of the Na-cellulose 004 reflection in the single

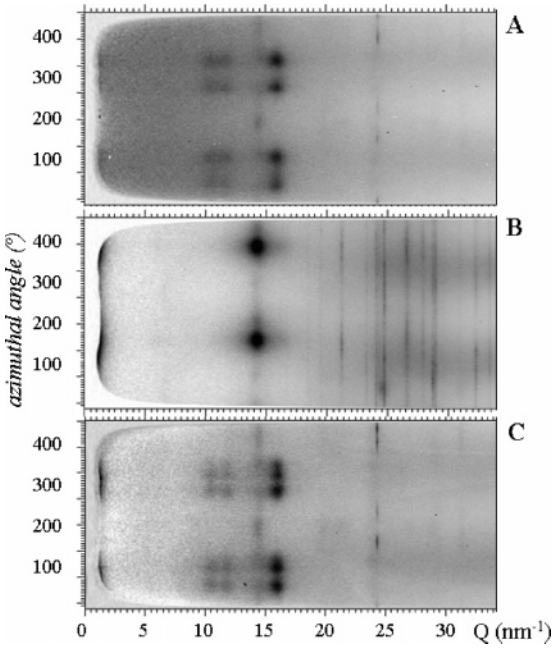

Figure 10. (A) Virgin cotton fiber pattern. (B) Pattern of cotton fiber after immersion in 5 N NaOH. (C) Cotton fiber after reaction with 5 N NaOH (B) and subsequent immersion in 0.5 N HCl.

phase range corresponds to a fiber repeat of 1.02 nm, in good agreement with previous studies of Na-cellulose I.[2,7] There was no evidence for a larger meridional spacing corresponding to Na-cellulose II.[2] If the 004 layer line position is compared against the fiber repeats reported for different Na-cellulose phases (Figure 8), only the formation of Na-cellulose I can be accommodated.

In summary, the results suggest that the tension applied to the fiber[2] and the increase in NaOH concentration during H_2O evaporation have led to the formation of Na-cellulose I. The linear increase in the intensity of the Na-cellulose 200 reflection suggests a gradual increase in NaOH concentration due to H_2O evaporation and hence a considerable stoichiometry range of NaOH in Na-cellulose I. This can be qualitatively understood with a straightforward model describing a shifting NaOH concentration gradient, as shown in Figure 9. The model assumes that the NaOH concentration at the Na-cellulose phase boundary is static and conforms to a Gaussian distribution while the macrodrop volume remains constant ($t = 0$). However, upon the cessation of microdropping, the macrodrop's volume becomes reduced by evaporation as it is no longer being replenished ($t > 0$). This results in a phase boundary shift toward the macrodrop (corresponding to a shift in the model's Gaussian distribution), the magnitude of which is essentially a function of t. Assuming the intensity of the Na-cellulose 200 reflection is proportional to NaOH concentration, its intensity at any position along the fiber can therefore be approximated by integration. This provides the good fit to the experimental data, shown by the solid line in Figure 6C.

Exposure of Na-Cellulose Containing Fiber to H_2O and HCl. Depending upon the solvents and swelling condition, various interconversion schemes involving different Na-cellulose phases and cellulose I/II phases have been proposed.[2,35] Thus, a complete reversibility of Na-cellulose I formation can be observed for cotton fibers freely immersed in aqueous NaOH (Figure 10). The split fiber pattern of the reformed cellulose suggests that the internal fiber structure has not been destroyed by this treatment as has also been observed by optical microscopy for other solvents.[36] However, unlike bulk immersion, the fiber in a microdrop setup is only locally targeted and therefore remains permeable to H_2O vapor. It is therefore of interest to study the stability of Na-cellulose in such a situation. Two such cases are reported: (i) exposure of the macrodrop to H_2O microdrops, which does not change the overall NaOH content in the system but provides a dilution followed by H_2O evaporation; (ii) exposure of the macrodrop to HCl microdrops, which reduces in addition to a transient dilution the overall NaOH content by the formation of NaCl

The effect of H_2O was explored by exposing the fiber containing Na-cellulose (analyzed already in Figure 4A) to a stream of H_2O microdrops for 30 min at the position of the aqueous NaOH macrodrop. A second mesh-scan with identical step-width and measuring time was then performed. Figure 11A corresponds to the azimuthally averaged patterns after NaOH exposure of the fiber already shown in Figure 4A. Figure 11B corresponds to the H_2O-washed fiber. The two consecutive mesh-scans have been aligned relatively to each other, as the scanned zones did not match directly. The influence of the dilution with H_2O can be readily seen in Figure 11B as the Na-cellulose 200 reflection has become weaker and more diffuse. This suggests that crystalline Na-cellulose domains have dissolved. Furthermore, the cellulose/Na-cellulose transformation zone has shifted by about 225 μm toward the macrodrop. This supports the assumption of a metastable Na-cellulose I phase, which can be converted back to cellulose I.[35,37] However, the observed shift of the transformation zone contrasts with electron diffraction studies which suggest that laterally compressed Na-cellulose I is converted back to cellulose I.[6]

The effect of HCl was explored by exposing a cotton fiber for about 30 min to 1 N NaOH microdrops, and then to a stream of 0.5 N HCl microdrops at the macrodrop position. The parameters of the subsequent mesh-scan were $15_h \times 3.5_v$ μm^2. Patterns were again summed in order to obtain a line of patterns along the fiber axis. It is interesting to note that patterns recorded at different positions along the fiber with both Na-cellulose and NaCl reflections show a strong difference in NaCl texture (Figure 12A). Thus, the NaCl reflections of the pattern at left show a powder texture while the reflection of the pattern to the right shows a fiber texture.

A composite image corresponding to the sequence of azimuthally integrated intensity distributions covering the most intense cellulose I and Na-cellulose I reflections is shown in Figure 12B. A cellulose/Na-cellulose transformation zone is observed, which resembles the composite image of the NaOH reacted fiber in Figure 5. The different NaCl textures of Figure 12A can be localized from a composite image showing the sequence of the azimuthal intensity distribution of the NaCl 200 reflection. (Figure 12C). The NaCl fiber texture is found in a zone of about 105 μm width close to the macrodrop, followed by a NaCl powder texture. The NaCl fiber texture suggests that only part of the intercalated NaOH has reacted with HCl so that NaCl has precipitated epitaxially on the fibrillar Na-cellulose domains. This is supported by a NaCl particle size of $L \approx 28$ nm, which corresponds roughly to the particle size of the Na-cellulose domains in the fiber direction (Figure 8). In addition, the azimuthal width of the 200 reflection agrees to the azimuthal width of the Na-cellulose 200 reflection. The random NaCl texture can be tentatively attributed to NaCl, which has been formed through dissolution of Na-cellulose domains followed by a growth process of cellulose domains with a random precipitation of NaCl crystallites in the fiber. This suggests also a shift of the phase transformation zone closer to the macrodrop, as already observed for H_2O-washing. The less constrained

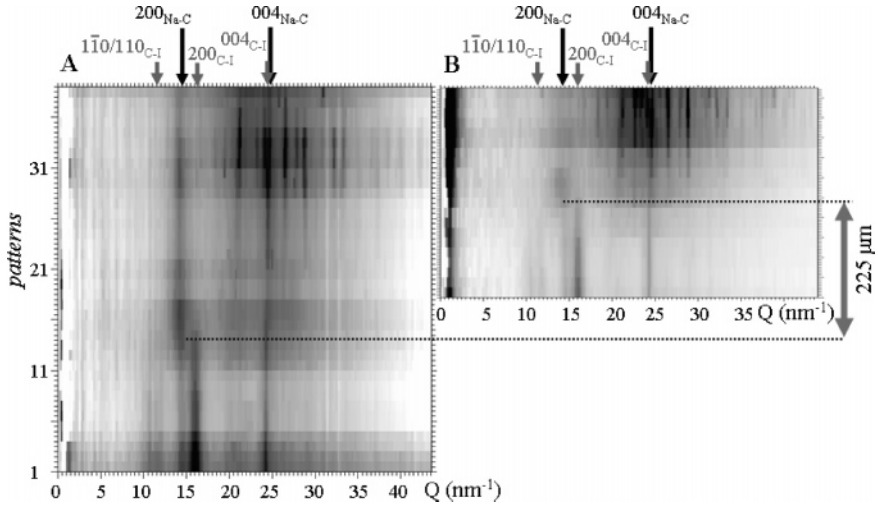

Figure 11. (A) Composite image of fiber after reaction with 1 N NaOH microdrops (same as for Figure 4A). (B) Composite image for same fiber but after exposure to H_2O microdrops. The two composite images were matched along the fiber axis as the scan-ranges were different. Note that the Na_2CO_3 peaks are at about the same position for the two composite images. The phase transformation zone has been shifted after H_2O-washing by about 225 μm toward the macrodrop.

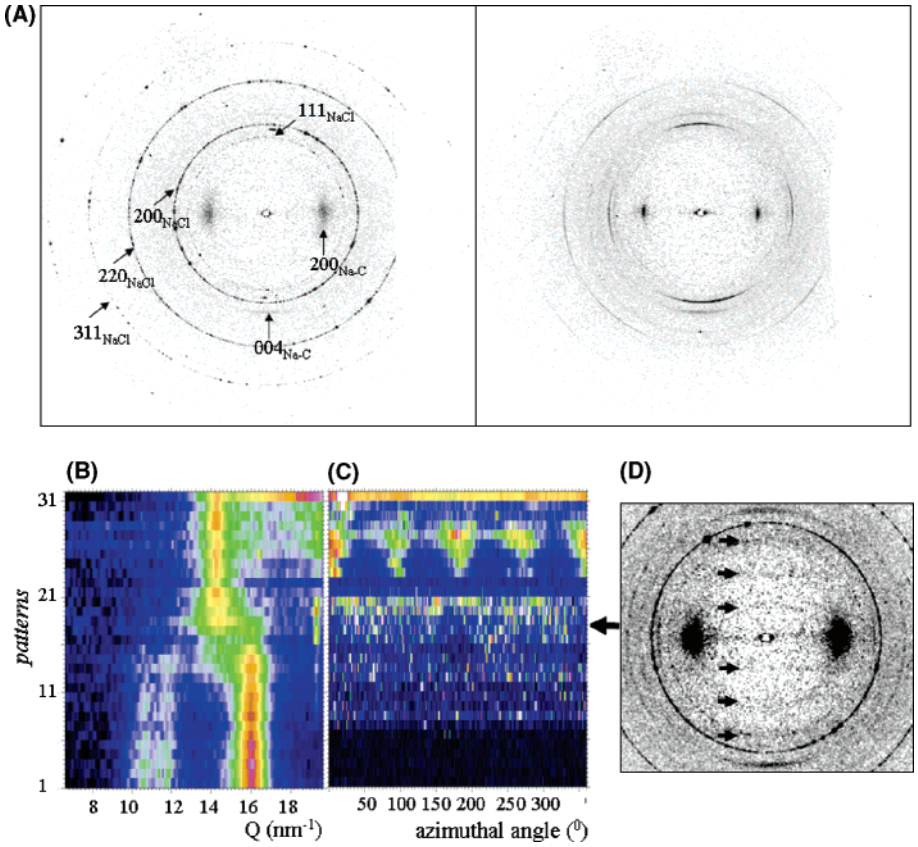

Figure 12. Cotton fiber after exposure to 1 N NaOH microdrops and subsequent reaction with 0.5 N HCl microdrops. (A) Two patterns recorded at different positions along the fiber showing both Na-cellulose I and NaCl reflections (with Miller's indices). The NaCl reflections on the left show a powder texture while the NaCl reflections on the right show a fiber texture. (B) Composite image of sequence of azimuthally averaged patterns, which cover the range of the main equatorial cellulose I and Na-cellulose I reflections. The sequence of patterns was obtained by summing patterns normal to the fiber axis (see Figure 5 and text; pattern 31 corresponds to the edge of the macrodrop). (C) Composite image of the radially averaged patterns across the 200 reflection of NaCl. (D) Pattern from middle of cellulose/Na-cellulose transformation zone, showing weak layer lines (arrows).

growth process of NaCl domains in the zone where cellulose domains are formed is reflected in a larger NaCl particle size of $L \approx 55$ nm. No evidence for a further phase was obtained from this study. Weak layer lines observed for a single pattern from the middle of the phase transformation zone agree to the fiber period of 1.01 ± 2 nm of Na-cellulose I[3] (Figure 12.D).

Conclusion and Outlook

It has been shown that the conversion of cellulose I into Na-cellulose I can be studied at the level of single cotton fibers using microdiffraction experiments. Complementary morphological studies by micro-SAXS experiments are in principle

feasible.[38] The current data supports the proposed nucleation/growth process. However, the intensity decay of the cellulose 200 reflection across the transformation zone does not seem to correlate well with the appearance of the Na-cellulose I 200 reflection, which can be interpreted by the random intercalation of the cellulose I lattice by NaOH. This question, and the presence of other Na-cellulose phases, should be addressed by mapping the transformation zone with a higher spatial resolution and by obtaining better counting statistics using flash-freezing techniques.[19] The presence of amorphous phases could be addressed by complementary spectroscopic methods. Thus, in-situ microdiffraction experiments have recently been combined with a Raman microprobe using a common beam size of 1 μm.[39]

The experimental techniques discussed above have considerable development potential. For example, the use of multiple microdrop-heads could permit solvents to be rapidly switched or the concentration level to be locally tailored. In-situ structural information could also be obtained during operation of the microdrop generator.[18] This could allow the reaction front to be studied by sweeping it through the microbeam. Such developments will profit from a further reduction of radiation damage and an optimization of the reflection signal/noise ratio by more sensitive detectors. Routine use of microdrop generators for the generation of highly localized gradients in chemical potential could find a multitude of applications in the study of liquid/solid reactions.

Acknowledgment. Cotton bolls were kindly provided by Dr. H. Chanzy (Cermav Grenoble). We wish to thank Dr. S. Eichhorn (UMI Manchester) and Dr. A French (ARS New Orleans) for valuable discussions. Financial support of the European Commission FP6 Programme SAXIER is acknowledged.

References and Notes

(1) Nishimura, H.; Okano, T.; Sarko, A. *J. Appl. Polym. Sci.* **1987**, *33*, 855−866.
(2) Okano, T.; Sarko, A. *J. Appl. Polym. Sci.* **1984**, *29*, 4175−4182.
(3) Okano, T.; Sarko, A. *J. Appl. Polym. Sci.* **1985**, *30*, 325−332.
(4) Nishimura, H.; Okano, T.; Sarko, A. *Macromolecules* **1991**, *24*, 759−770.
(5) Warwicker, J. O.; Jeffries, R.; Colbran, R. L.; Robinson, R. N. *A Review on the Literature on the Effect of Caustic Soda and Other Swelling Agents on the Fine Structure of Cotton*; Shirley Institute: Manchester, 1966.
(6) Kim, N. H.; Sugiyama, J.; Okano, T. *Mokuzai Gakkaishi* **1990**, *36*, 120−125.
(7) Nishimura, H.; Okano, T.; Sarko, A. *Macromolecules* **1991**, *24*, 759−770.
(8) Nishimura, H.; Sarko, A. *Macromolecules* **1991**, *24*, 771−778.
(9) Nishimura, H.; Sarko, A. *J. Appl. Polym. Sci.* **1987**, *33*, 867−874.
(10) Fink, P.; Walenta, E.; Philipp, B. *Papier* **1999**, *53*, 25−31.
(11) Philipp, B.; Fink, H. P. *Polym. News* **1999**, *24*, 122−126.
(12) Crawshaw, J.; Bras, W.; Mant, R.; Cameron, R. E. *J. Appl. Polym. Sci.* **2002**, *89*, 1209−1218.
(13) Müller, M.; Czihak, C.; Vogl, G.; Fratzl, P.; Schober, H.; Riekel, C. *Macromolecules* **1998**, *31*, 3953−3957.
(14) Riekel, C. *Rep. Prog. Phys.* **2000**, *63*, 233−262.
(15) Müller, M.; Riekel, C.; Vuong, R.; Chanzy, H. *Polymer* **2000**, *41*, 2627−2632.
(16) Moss, C. E.; Butler, M. F.; Mueller, M.; Cameron, R. E. *J. Appl. Polym. Sci.* **2002**, *83*, 2799−2816.
(17) Lee, E. R. *Microdrop Generation*; CRC Press: Boca Raton, FL, 2003.
(18) Rössle, M.; Flot, D.; Engel, J.; Riekel, C.; Chanzy, H. *Biomacromolecules* **2003**, *4*, 981−986.
(19) Lemke, H.; Burghammer, M.; Flot, D.; Roessle, M.; Riekel, C. *Biomacromolecules* **2004**, *5*, 1316−1324.
(20) Riekel, C.; Burghammer, M.; Flot, D.; Rössle, M. *Fibre Diffr. Rev.* **2004**, *12*, 36−40.
(21) Dinand, E. *Cellulose* **2002**, *9*, 7−18.
(22) David, C.; Noehammer, B.; Ziegler, E. *Microelectron. Eng.* **2002**, *61*−*62*, 987−992.
(23) Schroer, C. G., Kuhlmann, M., Lengeler, B., Günzler, T. F., Kurapova, O., Benner, B., Rau, C., Simionovici, A. S. In *Design and Microfabrication of Novel X-Ray Optics*; Snigirev, A., Snigireva, I., Mancini, D. C., Eds.; *SPIE Proceedings*, 2002; Vol. 4783, pp 10−18.
(24) Perrakis, A.; Cipriani, F.; Castagna, J. C.; Claustre, L.; Burghammer, M.; Riekel, C.; Cusack, S. *Acta Crystallogr.* **1999**, *D55*, 1765−1770.
(25) Hammersley, A. 2006, In http://www.esrf.fr/computing/scientific/FIT2D/.
(26) Davies, R. *J. Appl. Crystallogr.* **2006**, *39*, 267−272.
(27) Klug, H. P.; Alexander, L. E. *X-ray diffraction procedures for polycrystalline and amorphous materials*, 2nd ed.; Wiley-Interscience: New York, 1974.
(28) Meyer, K. H.; Misch, L. *Helv. Chim. Acta* **1937**, *20*, 232−244.
(29) Gancy, A. B. *J. Chem. Eng. Data* **1963**, *8*, 301−306.
(30) Wada, M.; Okano, T.; Sugiyama, J. *Cellulose* **1997**, *4*, 221−232.
(31) Burghammer, M.; Müller, M.; Riekel, C. In *Recent Research Developments in Macromolecules*; Pandalai, S. G., Ed.; Research Signpost: Trivandrum, India, 2003; Vol. 7.
(32) Nishiyama, Y.; Kuga, S.; Okano, T. *J. Wood Sci.* **2000**, *46*, 452−457.
(33) Irklei, V. M.; Goikhman, A. S. *Fibre Chem.* **1988**, *20*, 1−7.
(34) Isogai, A.; Agarwal, U. P.; Atalla, R. H. In *12th ISWPC International Symposium on Wood and Pulping Chemistry*; University of Wisconsin−Madison, Department of Forest Ecology and Management: Madison, Wisconsin, 2003; Vol. III, pp 263−266.
(35) Hayashi, J.; Yamada, T.; Kimura, K. *J. Appl. Polym. Sci. Symp.* **1976**, *28*, 713−727.
(36) deGruy, I. V.; Carra, J. H.; Goynes, W. R. In *Fiber Science Series*; O'Connor, R. T., Ed.; Marcel Dekker: New York, 1973; Vol. 1.
(37) Kim, N. H.; Sugiyama, J.; Okano, T. *Mokuzai Gakkaishi* **1991**, *37*, 637−643.
(38) Riekel, C.; Burghammer, M.; Müller, M. *J. Appl. Crystallogr.* **2000**, *33*, 421−423.
(39) Davies, R.; Burghammer, M.; Riekel, C. *Appl. Phys. Lett.* **2005**, *87*, 264105-1−264105-3
(40) Sobue, H.; Kiessig, H.; Hess, K. *Z. Phys. Chemie, Abt. B* **1939**, *43*, 309−328.

BM060844W